ORIGINAL ARTICLE

In silico studies of green fluorescent protein-tagged Hsp27-HPV16 E7 fusion protein and evaluation of cytokine secretion from antigen-presenting cells exposed to the fusion protein-carrying tumor-derived exosomes

Fatemeh Rezaei[1], Arash Arashkia[2], Fatemeh Fotouhi[3], Azam Bolhassani[1], Seyed Mehdi Sadat*[1]

[1] *Department of Hepatitis and AIDS, Pasteur Institute of Iran, Tehran, Iran*
[2] *Department of Molecular Virology, Pasteur Institute of Iran, Tehran, Iran*
[3] *Influenza and Respiratory Viruses Department, Pasteur Institute of Iran, Tehran, Iran*

Received: November 10, 2024 **Accepted:** December 9, 2024 **Online Published:** December 16, 2024
DOI: 10.5430/jst.v14n1p45 **URL:** https://doi.org/10.5430/jst.v14n1p45

ABSTRACT

Objective: Exosome (Exo)-based therapies have attracted considerable interest due to their potential as carriers for therapeutic molecules and their capacity to elicit anti-tumor immune responses. The objective of this study was to engineer TC-1 tumor cell line-derived exosomes with GFP-tagged heat shock protein (Hsp) 27-human papillomavirus (HPV)16 E7 fusion protein and evaluation of cytokine secretion from antigen-presenting cells (APCs: macrophages and dendritic cells) exposed to the engineered exosomes in vitro.

Methods: In this study, different in silico methods were employed to evaluate the Hsp27-E7 and Hsp27-E7-GFP fusion proteins as potential vaccine candidates. Regarding to the in silico data, the Hsp27-E7-GFP fusion gene was subcloned into pCDH lentiviral vector for production of lentivirions harboring the Hsp27-E7-GFP fusion protein in eukaryotic cells. Subsequently, the TC-1 tumor cells were transduced with these lentivirions to isolate the engineered exosomes (i.e., Exo-Hsp27-E7-GFP) using the ExoQuick-TC^{TM} kit and their characterization using physicochemical methods. Finally, the secretion of key cytokines (IFN-γ, TNF-α, and IL-10) was evaluated through incubation of antigen-presenting cells (APCs) with the engineered Exo-Hsp27-E7-GFP using enzyme-linked immunosorbent assay (ELISA).

Results: Our *in silico* data showed that both the Hsp27-E7 and Hsp27-E7-GFP constructs were soluble and non-allergenic, and exhibited strong interaction with TLR4. Indeed, the linkage of GFP did not affect the physicochemical properties, and interaction of Hsp27-E7 with the immune receptors. Moreover, western blot analysis confirmed the presence of Hsp27-E7-GFP fusion protein in the isolated exosomes. The Exo-Hsp27-E7-GFP could significantly enhance the secretion of TNF-α and IL-10 from APCs compared to Exo and Exo-GFP, as well.

Conclusions: These engineered vesicles derived from tumor cells demonstrate the capacity to induce effective immunity, suggesting their potential as a promising strategy in the development of cell-free vaccine candidates.

Key Words: Human papillomavirus 16, E7 oncoprotein, Heat shock protein 27, Green fluorescent protein, Exosome, Immunostimulatory effects

*Correspondence: Seyed Mehdi Sadat; Email: mehdi_sadat@pasteur.ac.ir; Address: Department of Hepatitis and AIDS, Pasteur Institute of Iran, Tehran, Iran.

1. INTRODUCTION

Human papillomavirus (HPV) infection is a significant global health concern, particularly due to its association with various cancers, including cervical cancer.[1] Persistent high-risk HPV infection is a key factor in cervical precancerous lesions and cancer, with about 70% of cases linked to oncogenic HPV types 16 and 18.[2] Despite advancements in screening and vaccination efforts, HPV-related cancers continue to pose a challenge, underscoring the urgent need for innovative treatment strategies.[3,4] The HPV oncoproteins E6 and E7 are instrumental in oncogenesis, disrupting normal cell cycle regulation and leading to uncontrolled cell proliferation.[5] While preventive vaccines have shown efficacy in reducing HPV infections, they are less effective for individuals with pre-existing lesions or established cancers.[6,7] Consequently, there is an increasing focus on developing therapeutic vaccines that can elicit robust immune responses against cells expressing HPV oncoproteins.[8]

Extracellular vesicles (EVs), particularly exosomes, have emerged as promising platforms for cancer immunotherapy due to their ability to modulate immune responses and transport antigenic material.[9] Exosomes facilitate the presentation of tumor-associated antigens to immune cells, thereby enhancing the immune response against tumors.[10] Heat shock proteins (HSPs), such as Hsp27, play a vital role in this process by acting as chaperones that assist in loading tumor antigens into exosomes.[11–13] This mechanism not only enhances antigen presentation but also stimulates immune responses, making HSPs as valuable components in the design of therapeutic vaccines.[14] On the other hand, green fluorescent protein (GFP) is widely utilized as a reporter molecule for detection of gene expression and protein localization in vitro or in vivo. Moreover, some studies showed that GFP could elicit an immune response in various models. Indeed, GFP induced T-cell-mediated immunogenicity through MHC class I presentation, leading to cytotoxic T-lymphocyte recognition and rejection of GFP-expressing cells.[15] The extent of GFP immunogenicity can vary depending on the animal strain, route of administration, and immunosuppressant use.[15] Additionally, GFP expression was found to influence tumor growth and metastasis in mouse models.[16]

In this study, TC-1 mouse lung cancer cell line, a widely used model for studying HPV-related cancers,[17] were transduced with lentivirions harboring GFP-tagged Hsp27-HPV16E7 fusion protein. Then, the Hsp27-E7-GFP-carrying exosomes were isolated and characterized with different methods (named as Exo-Hsp27-E7-GFP). The immunostimulatory effects of the engineered exosomes were investigated by cytokines assay after their incubation with antigen presenting cells (APCs) including macrophage and dendritic cells (DCs) in vitro. This approach may provide valuable insight into the potential of engineered exosomes as a therapeutic strategy against HPV-related tumors. Indeed, the findings of study can provide a comprehensive understanding whether GFP tagging influences the immunogenic potential of the Hsp27-E7 fusion protein delivered via engineered exosomes or not. Overview of this study was shown in a graphical abstract for further clarification (see Figure 1).

2. METHODS

2.1 Study design

A multidisciplinary approach that integrates bioinformatics, molecular modeling, and experimental techniques, has been used in the current study. In the first phase, we conducted molecular docking simulations with toll-like receptors (TLRs) and HSP-specific receptors to predict immune interactions, alongside 100-nanosecond molecular dynamics simulations to evaluate the structural stability of fusion proteins. For the experimental phase, we employed the engineered lentivirions containing Hsp27-E7-GFP fusion protein to transduce the TC-1 tumor cell line and subsequently isolate exosomes from the transduced cells. The isolated exosomes were incubated with murine APCs to assess their ability in stimulation of cytokine production. This evaluation is crucial for understanding how engineered exosomes can stimulate immune responses and contribute to therapeutic strategies against HPV-related cancers. This study builds on our previous research that Hsp27-based constructs, particularly full-length ones (e.g., Hsp27-E7 protein), strongly interacted with immune receptors, suggesting their potential to trigger a robust immune response.[18] Herein, we sought to investigate the potential of GFP as both an immunostimulant and a tracking marker within the context of Hsp27-E7 protein in exosome-based construct.

2.2 In silico studies

Various bioinformatics tools were used to compare some physicochemical and immunostimulatory properties of the full-length Hsp27-E7 and Hsp27-E7-GFP fusion proteins as follows. The protein sequences for mouse HSP27 (P14602), HPV16 E7 (P03129), and GFP (P42212) were obtained from the UniProt server (`https://www.uniprot.org/`).

2.2.1 *Tertiary structure modeling, refinement, and validation*

To model the 3D structures of the constructs, we utilized the RoseTTAFOLD tools available on the Robetta server (`https://robetta.bakerlab.org/`). RoseTTAFOLD employs a deep learning-based method, TrRosetta, known for its speed and accuracy.[19] The Robetta server generated five models for each construct. These initial models were then refined us-

ing the GalaxyRefine 2 server (http://galaxy.seoklab.org/cgi-bin/submit.cgi?type=REFINE2) to further enhance structural quality. GalaxyRefine 2 implements short molecular dynamics simulations and side-chain repackaging to improve model stability.[20] The quality of the refined structures was assessed using the SAVE5.0 server (https://servicesn.mbi.ucla.edu/SAVES/).[21,22] We analyzed the Ramachandran diagram using PROCHECK to assess the favored, allowed, and disallowed regions of the backbone dihedral angles, indicating the quality of the modeled structure. ERRAT calculates an overall quality score, with higher scores indicating better model quality.

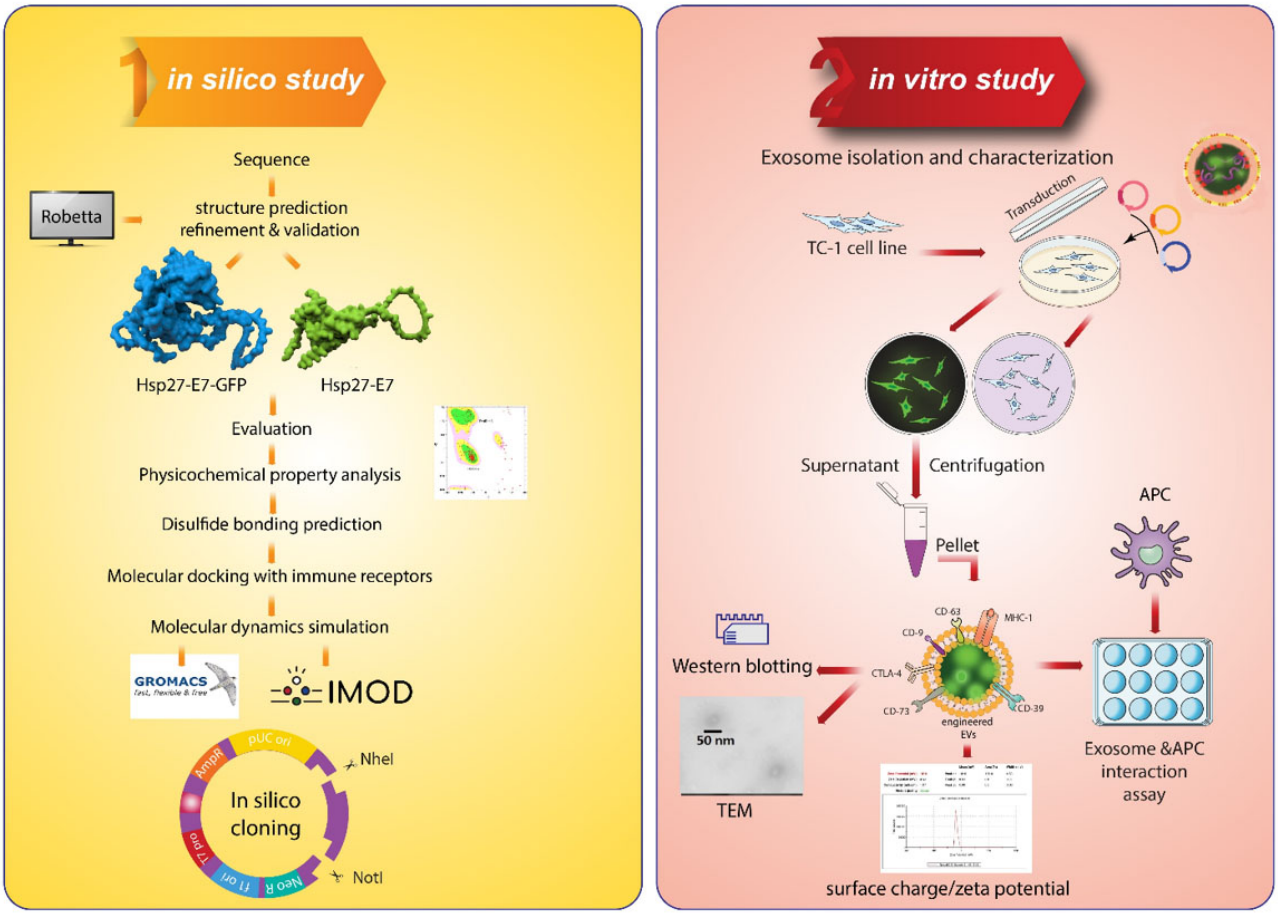

Figure 1. Graphical abstract: Overview of this study
Created in BioRender. Fontana, T. (2024) https://BioRender.com/a23j248

2.2.2 *Molecular docking with immune receptors*

We conducted molecular docking simulations to investigate the potential interactions of our vaccine constructs with key immune receptors. We focused on receptors involved in both innate and adaptive immunity, including TLR2, TLR3, TLR4, TLR5, TLR7, and TLR8 (for innate immunity), and scavenger receptor expressed by endothelial cells-1 (SREC-1), CD14, lectin-like oxidized low-density lipoprotein receptor-1 (LOX-1) (for adaptive immunity). Receptor structures were obtained from the Protein Data Bank (PDB) (http://www.rcsb.org/). Molecular docking was performed using the HDock server (https://http://hdock.phys.hust.edu.cn/), which predicts based on a hybrid algorithm of template-based modeling and ab initio free docking. Finally, the LigPlot+ software was used to visualize the interactions between the fusion proteins and TLR4, highlighting the specific amino acids involved in complex formation.

2.2.3 *Physicochemical property analysis*

To determine the physical and chemical properties of the designed constructs, we employed the ProtParam online server (https://web.expasy.org/protparam/). This server provided multiple physicochemical parameters, including molecular weight, isoelectric point (pI), instability index (II), and grand average of hydropathicity (GRAVY). The molecular weight (MW) and theoretical pI were calculated by ProtParam. The instability index (II) was determined based

on dipeptide instability values, providing an estimate of the protein's inherent stability. GRAVY, calculated using hydropathic values of all amino acids, indicates the amphipathic nature of a protein; negative and positive values suggest a hydrophilic or hydrophobic nature, respectively.[23] To evaluate the allergenicity of fusion proteins, we utilized the AllerTop v. 2.0 server (https://www.ddg-pharmfac.net/AllerTOP/index.html). Protein solubility is critical for industrial and therapeutic applications. We used the Protein-Sol server (https://protein-sol.manchester.ac.uk/) to predict the protein solubility. A QuerySol score greater than 0.45 suggests that proteins are more soluble than average.[24]

2.2.4 *Disulfide bonding prediction*

To anticipate disulfide bond formation, we used the DIpro scratch protein predictor server (http://scratch.proteomics.ics.uci.edu/). This tool is specifically designed to predict protein structural features, including disulfide bridges. It was selected for its reliability in determining the presence or absence of disulfide bonds, estimating their quantity, and predicting the bonding state of each cysteine residue with paired bonds. The predictor demonstrates an accuracy of 85% and a recall rate of 90%.[25] DIpro integrates 2D-RNN architectures with support vector machines (SVMs) to differentiate proteins that have disulfide bonds from those that do not. It also uses graph matching algorithms to effectively match cysteine residues.[26,27]

2.2.5 *Molecular dynamics simulation*

To investigate the dynamic stability and interactions of the validated protein structures with TLR4, we conducted molecular dynamics (MD) simulations using GROMACS v5.0. This open-source software is widely utilized for dynamic simulations of biomolecules and provides a comprehensive suite for system preparation, simulation, and analysis tools. The simulation began with preparing the validated protein-TLR4 complex structure, which was solvated using the SPCE water model and electro-neutralized with appropriate ions. Energy minimization was conducted using the steepest descent algorithm to eliminate any initial unfavorable contacts. Following this, the system underwent equilibration in two phases. The first phase involved a 100 ps equilibration run under constant volume and temperature (NVT) conditions at 310 K, utilizing a Nose-Hoover thermostat. This was followed by a second phase, where another 100 ps run was conducted under constant pressure and temperature (NPT) conditions at 310 K and 1 bar, employing a Parrinello-Rahman barostat. Once equilibration was complete, we carried out a 100 ns MD simulation of the complex using the leap-frog algorithm. The resulting trajectory was then analyzed using standard MD metrics. We assessed the overall stability of the complex through root mean square deviation (RMSD), identified regions of flexibility within the complex using root mean square fluctuation (RMSF), and evaluated the compactness and structural integrity of the complex by calculating the radius of gyration (Rg). This comprehensive approach provides valuable insights into the dynamic behavior and stability of the protein structure in its interaction with TLR4.

2.2.6 *Normal mode analysis*

To characterize the dynamic flexibility of the vaccine-receptor complex, we employed normal mode analysis (NMA) using the iMODS server (http://imods.chacon lab.org/).[28] NMA is a technique that describes the collective motions of a protein around its equilibrium structure, providing insights into its dynamic behavior.[29] While MD simulations can explore a larger conformational space, NMA offers a computationally efficient method for identifying key flexible regions.[30,31] The iMODS server utilizes NMA in internal (dihedral) coordinates, which is particularly well-suited for analyzing the collective motions of macromolecules.[32] This server generates a range of outputs, including deformability, B-factor, eigenvalues, variance, covariance maps, and elastic networks, which provide insights into the complex's flexibility and potential for conformational changes.[32] We leveraged these outputs to analyze the proteins' flexibility in relation to its interaction with TLR4, focusing particularly on eigenvalues that show the rigidity of the system.

2.2.7 *In silico cloning*

In our computational analysis, we found no significant differences between two fusion constructs (Hsp27-E7 and Hsp27-E7-GFP) in terms of their docking with receptors, dynamic stability, flexibility, and other features. Given the findings from other studies highlighting the importance of GFP as an immune modulator,[15] we opted to evaluate the GFP-tagged construct in the experimental phase. This evaluation will allow us to assess the functionality of the engineered Hsp27-E7-GFP exosome. Thus, the Hsp27-E7-GFP fusion gene was successfully cloned into the pCDH-CMV-MCS-EF1α-Puro lentiviral vector (Catalog number CD510B-1; System Biosciences; USA) using SnapGene software (version 5.2.3) (https://www.snapgene.com/).

2.3 Experimental studies

2.3.1 *Vector design and construction*

The Hsp27-E7 fusion gene was constructed by amplifying the HPV16 E7 gene from pQE30-E7 using Pfu DNA polymerase (Fermentas, Germany) and ligating it into the linearized pET24a (+)-Hsp27 vector. Both constructs were previously prepared by our group. The fusion construct was verified by PCR, restriction digestion with EcoRI/SalI (Fermentas, Germany), and Sanger sequencing. Then, the Hsp27-

E7 fusion gene was ligated to the GFP sequence within pEGFP.N3, creating the Hsp27-E7-GFP fusion construct. The Hsp27-E7-GFP gene was subcloned from pEGFP.N3-Hsp27-E7 into the pCDH lentiviral vector using NheI/NotI enzymes (Fermentas, Germany), preparing it for gene delivery. The pCDH-Hsp27-E7-GFP was purified using a plasmid Giga kit (Qiagen, Germany) and quantified by NanoDrop spectrophotometry. Moreover, the psPAX2 and pMD2.G vectors (System Biosciences; USA) were purified from DH5α *E. coli* to prepare the recombinant lentiviral particles.

2.3.2 *Lentiviral particles production and characterization*

Lentiviral particles were generated by co-transfecting Lenti-X^{TM} 293T cells with the pCDH-Hsp27-E7-GFP (or pCDH-GFP; Catalog number CD513B-1; pCDH-CMV-MCS-EF1α-Green Puro; System Biosciences; USA), psPAX2, and pMD2.G packaging plasmids using TurboFect^{TM} reagent (Fermentas, Germany). Supernatants containing the lentiviral particles were harvested at different time intervals after transfection (24 h, 48 h and 72 h) and concentrated through high-speed centrifugation. Transfection efficiency was measured by quantifying the percentage of cells that expressed the Hsp27-E7-GFP fusion protein using fluorescent microscopy and flow cytometry. The multiplicity of infection (MOI) was determined by diluting the concentrated virions and assessing the percentage of GFP-positive cells through flow cytometry, following a formula previously outlined by Zhang et al.[33] An optimal MOI of 20 was established to achieve high transduction efficiency.

2.3.3 *Transduction of TC-1 cell line with lentivirions*

The TC-1 cell line was transduced with the lentivirions containing Hsp27-E7-GFP or GFP in the presence of polybrene (8 μg/mL) to enhance transduction efficiency. Transduction was confirmed by comparing the GFP expression levels in transduced and non-transduced cells using fluorescent microscopy and flow cytometry. These cells served as a valuable tool for isolating exosomes in subsequent experiments.

2.3.4 *Exosome isolation and characterization*

This study sought to isolate and characterize exosomes derived from TC-1 cells expressing the Hsp27-E7-GFP fusion protein (Exo-Hsp27-E7-GFP). To achieve this, we employed the ExoQuick-TC^{TM} kit (System Biosciences, USA) for exosome isolation as the optimal technique. This kit facilitated rapid and gentle exosome isolation, crucial for preserving the integrity of the engineered exosomes. Supernatants from non-transduced TC-1 cells, and those transduced with either lentivirion harboring the pCDH-GFP or lentivirions harboring the pCDH-Hsp27-E7-GFP, were processed using the ExoQuick-TC^{TM} kit (named as Exo, Exo-GFP and Exo-Hsp27-E7-GFP, respectively). Exosome quantification was carried out using a bicinchoninic acid (BCA) assay kit (Parstous, Iran). Furthermore, transmission electron microscopy (TEM) was utilized to visualize the morphology and size of the isolated exosomes. The zeta potential of the isolated exosomes was determined using a Zetasizer Nano ZSP (Malvern Instruments), providing information about their surface charge.

To confirm the presence of exosomal markers and the transduced proteins within the isolated exosomes, western blotting was performed. The membrane was probed with primary antibodies against the exosomal markers CD63 (1:5,000 v/v; Abcam, USA) and CD9 (1:500 v/v; Abcam, USA), and subsequently with a secondary HRP-conjugated antibody (total IgG, 1:10,000 v/v; Sigma, Germany). To assess the presence of the desired transduced proteins, the membrane was probed with HRP-conjugated polyclonal GFP antibody (1:5,000 v/v; Abcam, USA).

2.3.5 *Exosome-APC interaction assay*

To assess the immunostimulatory properties of the engineered exosomes harboring Hsp27-E7-GFP (Exo-Hsp27-E7-GFP), we investigated their effects on APCs. Firstly, dendritic cells were isolated from the bone marrow of naïve C57BL/6 mice (n = 4; 5-7-week-old; Pasteur Institute of Iran) and cultured in complete RPMI medium (20% FBS) supplemented with GM-CSF (20 ng/mL) and IL-4 (10 ng/mL) (PeproTech; USA), as described in our previous study.[34] These DCs (5×10^5 cells/well) were then seeded in a 24-well plate, and individually incubated with 20 μg of each antigen candidate including Exo-Hsp27-E7-GFP, Exo-GFP, and Exo. The cells were incubated for 48 h at 37°C and 5% CO_2, and the levels of IL-10, TNF-α, and IFN-γ were measured using a sandwich ELISA kit (Mabtech; Sweden). Untreated DCs served as a negative control.

Additionally, macrophages (RAW 264.7 cell line) were cultured in DMEM supplemented with 10% FBS and 1% penicillin-streptomycin at 37°C in a humidified atmosphere with 5% CO_2. Cells were seeded in 24-well plates at a density of 1×10^5 cells/well and allowed to adhere overnight. The following day, cells were treated with Exo-Hsp27-E7-GFP, Exo-GFP, and Exo, individually. Untreated macrophages served as a negative control. After 48 h incubation, the cell culture supernatants were collected and analyzed for TNF-α, and IFN-γ, and IL-10 production using a sandwich ELISA kit (Mabtech; Sweden), according to the manufacturer's instructions. It should be mentioned that in vitro studies were conducted in strict adherence to approved protocols and in compliance with the highest standards of animal care at the Pasteur Institute of Iran. This study was conducted in accordance with ethics code IR.PII.REC.1400.025.

2.3.6 *Statistical analysis*

Statistical analyses were performed by Prism software version 8 (GraphPad; USA) using one-way ANOVA test and was conducted to evaluate the differences among groups. The results were shown as mean ± standard deviation (SD) for each group, with a p-value less than 0.05 ($p < .05$) deemed statistically significant.

3. RESULTS

3.1 Bioinformatics studies

Comprehensive in silico analysis of Hsp27-E7-GFP fusion protein as a potential antigen candidate was performed as compared to Hsp27-E7 fusion protein for evaluating the physicochemical and immunostimulatory properties of Hsp27-E7 as well as the effects of GFP on these properties.

3.1.1 *3D structure modeling and validation*

Based on the final models generated by the RoseTTAFOLD server, Model 1 was selected for presentation, with Part I representing the Hsp27-E7 structure and Part II for the Hsp27-E7-GFP structure. The GalaxyRefine server results indicated the most refined model as illustrated in Fig 2A. For the Hsp27-E7 model, Ramachandran plot analysis indicated that a significant majority (86.3%) of protein residues adopted favored conformations, with the remaining residues distributed as follows: 12.2% additional allowed, 0.4% generously allowed, and 1.1% disallowed. (Part I in Fig 2B). In contrast, the analysis for the Hsp27-E7-GFP model showed 83.5% of residues in the favored region, 12.8% in additional allowed, 2.1% in generously allowed, and 1.6% in disallowed regions (Part II in Fig 2B). The ERRAT server, which evaluates non-bonded interactions, yielded scores of 78.235 for Part I and 73.731 for Part II (Fig 2C). Generally, an ERRAT score above 50 indicates good model quality.[35]

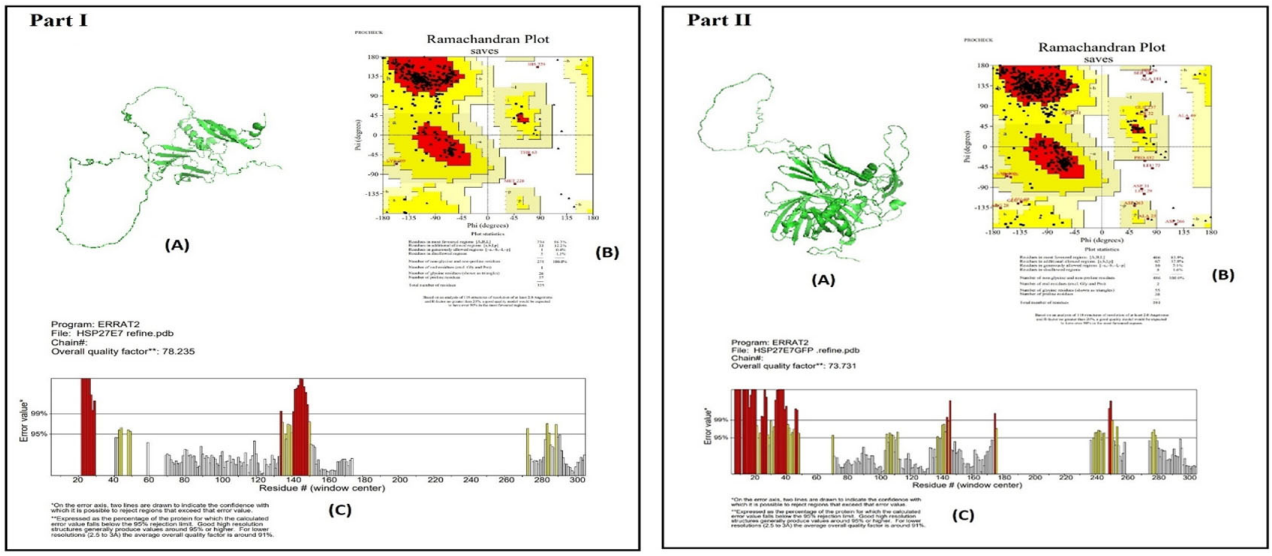

Figure 2. Final model and validation results

(A) Structure of the final model; (B) Ramachandran plot analysis, indicating that 86.3% of residues in Part I and 83.5% in Part II fall within the favored and allowed regions; (C) ERRAT plot demonstrates that the overall quality factor for the residues of the multi-epitope protein is 78.2% for Part I and 73.7% for Part II

3.1.2 *Molecular docking outcomes*

Among the evaluated TLRs, molecular docking results of the fusion proteins with TLRs and Hsp- specific receptors were obtained using the HDock server (see Table 1).

Docking analysis demonstrated that both the Hsp27-E7 and Hsp27-E7-GFP fusion proteins exhibited a strong affinity for TLR4, with docking scores of -294.94 and -286.96, respectively. This finding suggests a preferential engagement of these fusion proteins with TLR4, a critical receptor involved in innate immune responses. Moreover, the Hsp27-E7 and Hsp27-E7-GFP fusion proteins indicated a strong affinity for LOX-1 receptor with docking scores of -309.68 and -281.68, respectively as compared to other HSP-specific receptors. However, the linkage of GFP to the Hsp27-E7 fusion protein led to a considerable decrease in docking scores across Hsp-specific receptors, indicating that the presence of GFP may interfere with the binding of the fusion protein to its target receptors. The interaction between the fusion protein and TLR4 was visualized using LigPlot+ software (see Fig-

ure 3). The DIMPLOT program identified hydrogen bonds interactions. Specifically, residues Asp 59, Asp 83, Ser 85, Glu 134, His 158, Asp 208, Asp 264, Lys 263, Arg 337, Asp 41, Arg 233, and Arg 288 from TLR4 formed hydrogen bonds with Lys 109, Thr 112, Glu 111, Arg 106, Thr 115, Ser 103, Asp 101, Arg 68, Asp 100, and Asp 99 from the Hsp27-E7-GFP fusion protein. Analysis of the docking files using the PyMOL software revealed that both the Hsp27-E7 and Hsp27-E7-GFP constructs engage with TLR4 through amino acids situated in the N-terminal region of the Hsp27 sequence. Importantly, both constructs exhibited a comparable interaction pattern with TLR4, suggesting that the Hsp27 sequence is essential for mediating this interaction.

3.1.3 *Physicochemical properties*

Bioinformatics analysis of the Hsp27-E7 and Hsp27-E7-GFP fusion proteins revealed similar physicochemical properties, suggesting potential for efficient expression and functionality. The molecular weight of Hsp27-E7-GFP was significantly higher (63,925.55 Da) than Hsp27-E7 (35,537.70 Da) due to the added GFP tag, while both proteins exhibited comparable isoelectric points, indicating similar charge characteristics at physiological pH. The instability index suggested that both Hsp27-E7 and Hsp27-E7-GFP were stable proteins. Notably, both proteins were predicted to be non-allergenic, indicating potential safety for future applications. Additionally, their calculated solubility scores, 0.543 for Hsp27-E7 and 0.468 for Hsp27-E7-GFP, suggested that they were likely soluble in aqueous solutions, facilitating downstream applications (see Table 2). These bioinformatics predictions offer valuable insights for guiding future experimental efforts toward optimizing protein expression, purification, and functional characterization of these fusion proteins.

Table 1. Docking scores between final models of fusion proteins and receptors

Fusion protein	TLR2	TLR3	TLR4	TLR5	TLR7	TLR8	LOX-1	CD14	SREC-1
Hsp27-E7	-260.37	-294.44	-294.94	-284.59	-272.91	-301.25	-309.68	-294.14	-298.91
Hsp27-E7-GFP	-270.30	-283.68	-286.96	-286.86	-263.80	-267.21	-281.68	-275.27	-272

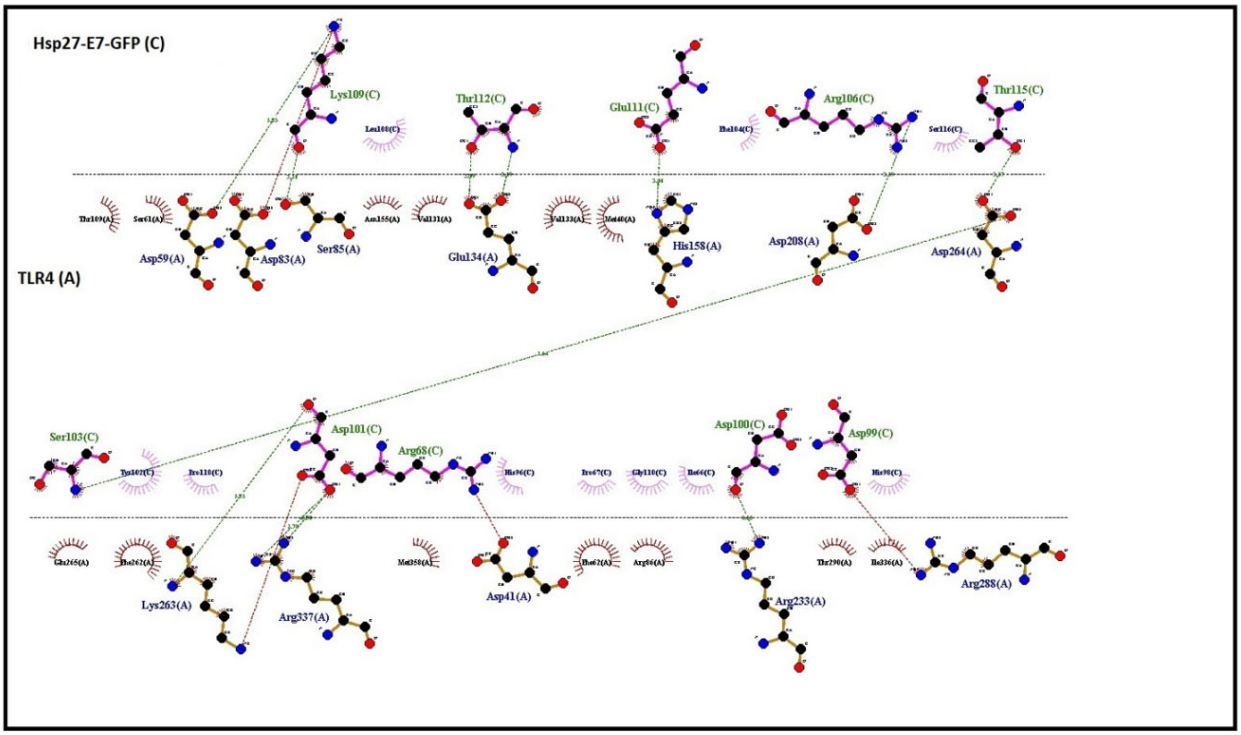

Figure 3. Schematic representation of the interaction between the fusion protein and TLR4 using LigPlot+ software

This figure shows residues involved in hydrophobic interactions, hydrogen bonds, and salt bridges in the best docked conformations; Green dashed lines represent hydrogen bonds in the Hsp27-E7-GFP/TLR4 complex

Table 2. Physicochemical characteristics of the fusion proteins

	MW	pI	Estimated half-life (hours)			II	Aliphatic index	GRAVY	Allergenicity	Solubility
			Mammalian reticulocytes	Yeast	*Escherichia coli*					
mHsp27-E7	35,537.70	5.01	30	> 20	> 10	37.25 (stable)	69.05	-0.471	Non-allergen	0.543 (soluble)
mHSP27-E7-GFP	63,925.55	5.31	30	> 20	> 10	34.53 (stable)	69.29	-0.513	Non-allergen	0.468 (soluble)

Note. MW: Molecular weight; II: Instability index; GRAVY: Grand average of hydropathicity

3.1.4 *Disulfide bonding prediction*

The disulfide bond connectivity of the Hsp27-E7 and Hsp27-E7-GFP constructs was predicted using the DIpro server, a component of the SCRATCH protein predictor suite. DIpro makes two independent predictions: first, it determines whether disulfide bonds are present in the protein, and second, it identifies the locations of those bonds.[27] In the case of the Hsp27-E7 fusion protein, the analysis revealed a total of 8 cysteine residues. Cysteines at positions 251, 285, 288, 295, 318, and 321 are likely to be involved in the formation of three disulfide bonds. The Hsp27-E7-GFP fusion protein possessed 10 cysteine residues. This prediction indicated that four disulfide bonds would be formed, involving cysteines at positions 251, 285, 288, 295, 318, 321, 391, and 413.

3.1.5 *Molecular dynamics analysis*

To determine the structural stability of the confirmed constructs (i.e., Hsp27-E7 and Hsp27-E7-GFP) and their interactions with TLR4, we conducted a 10-nanosecond molecular dynamics (MD) simulation. Analysis of the root mean square deviation (RMSD) of the trajectory revealed that the complex attained a stable state after approximately four nanoseconds. Further evaluations, including root mean square fluctuation (RMSF) and radius of gyration (Rg) analyses of the constructs within the TLR4, as well as the quantification of hydrogen bonds between the construct and receptor, demonstrated that the construct maintained stability during its interactions with the receptor.[36]

The stability of the backbone atoms is inversely proportional to the RMSD values; higher RMSD values indicate greater instability.[37] The first 20 nanoseconds of the simulation showed a typical RMSD increase as the proteins adjusted to the aqueous environment.[38] The Hsp27-E7-GFP/TLR4 and Hsp27-E7/TLR4 complexes reached equilibrium around 45 nanoseconds, displaying consistent behavior throughout the simulation duration. The average RMSD values for the Hsp27-E7-GFP/TLR4 and Hsp27-E7/TLR4 complexes were found to be 0.36 nm (ranging from 0.15 to 0.54 nm) and 0.4 nm (ranging from 0.25 nm to 0.55 nm), respectively. This suggests that both fusion protein constructs exhibit a stable interaction with TLR4, with minimal structural deviations observed throughout the simulations. The RMSD values for the Hsp27-E7-GFP/TLR4 complex (average 0.36 nm) were slightly lower than those observed for the Hsp27-E7/TLR4 complex (average 0.4 nm), indicating a potentially tighter and more stable interaction between the GFP-tagged fusion protein and TLR4. The consistent RMSD plateaus observed for each construct demonstrate that the structures settled into a stable average conformation, justifying the evaluation of local fluctuations (see Figure 4A).

Within the context of MD simulations, high RMSF values highlight regions with greater flexibility, while low RMSF values indicate regions that exhibit restricted movements.[37] Small proteins generally exhibit acceptable fluctuations when their RMSF values remain under 2Å. The comparison of fluctuations in the Hsp27-E7-GFP/TLR4 and Hsp27-E7/TLR4 complexes revealed that the presence of proline residues in the epitope sequence from residues 20 to 60 may have resulted in greater local flexibility variation in the RMSF values compared to the complete sequence. The RMSF plot depicted residual fluctuations in various regions of the protein for each construct. Also, beyond the N- and C-terminal residues, the regions spanning residues 625 to 734 in both Hsp27-E7-GFP/TLR4 and Hsp27-E7/TLR4 complexes exhibited the most significant dynamic fluctuations, with similar behaviors observed in the regions from 1,080 to 1,110 of the Hsp27-E7-GFP/TLR4 complex. The average RMSF values for the Hsp27-E7-GFP/TLR4 complex was 0.33 nm (ranging from 0.03 nm to 0.6 nm) and for the Hsp27-E7/TLR4 complex was 0.45 nm (ranging from 0.1 nm to 0.8 nm) (see Figure 4B).

The Rg values calculated from the MD trajectory reveal the protein's compactness and rigidity during the simulation. Higher Rg values suggest a more expanded, less compact structure, while lower Rg values point to a tighter, more stable configuration.[37] The Rg analysis indicated a greater degree of expansion in the Hsp27-E7-GFP/TLR4 complex compared to the Hsp27-E7/TLR4 complex, implying that the latter is more stable. The Hsp27-E7/TLR4 complex had an average Rg of 3.3 nanometers, with values ranging from 3.2 to 3.4 nanometers. In contrast, the Hsp27-E7-GFP/TLR4

complex had a larger average Rg of 3.63 nanometers, with values ranging from 3.58 to 3.68 nanometers. Rg plots revealed fluctuations of less than 2Å for all protein systems, providing evidence for their structural stability (see Figure 4C).

3.1.6 *Normal mode analysis*

The iMODS analysis revealed crucial insights into the dynamic behavior of the Hsp27-E7 and Hsp27-E7-GFP complexes when interacting with TLR4. Utilizing a coarse-grained alpha-carbon model, the Hsp27-E7-GFP analysis identified 1,248 model residues and 1,260 pseudo-atoms, with 2,416 dihedral angles contributing to the protein's flexibility. The eigenvalue spectrum indicated significant mobility, particularly in mode 5, which exhibited the highest deformability (5.728e-05), while mode 1 displayed the least deformability (9.345e-06). Additionally, the distance-covariance matrix revealed coupled motions between residue pairs, highlighting regions of correlated and anti-correlated dynamics. In a related analysis of the Hsp27-E7 complex with TLR4, a similar coarse-grained approach identified 970 model residues and 978 pseudo-atoms, with 1881 dihedral angles contributing to flexibility. The eigenvalue analysis in this case indicated significant mobility as well, particularly in mode 2, which exhibited the highest maximum mobility (2.975) and a maximum deformation value of 3.095e-05 (see Figure 5). The distance-covariance matrix further emphasized the coupled motions between residue pairs, revealing critical correlated and anti-correlated dynamics.

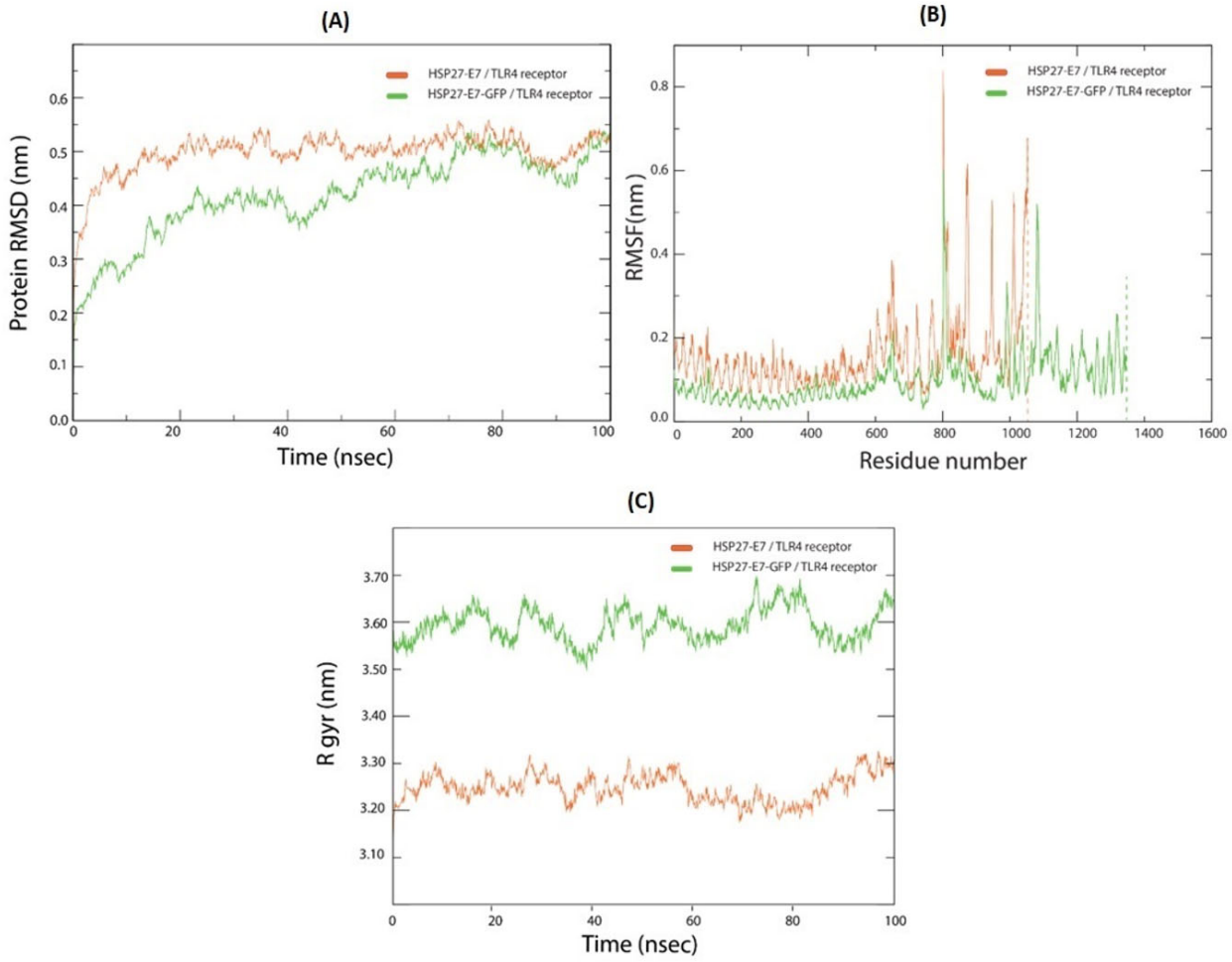

Figure 4. The RMSD (A), RMSF (B), and radius of gyration (Rg) (C) plots for the constructs in complex with TLR4 receptor: The data presented in these graphs indicate that the docked complexes achieved relative stability rapidly and exhibited no significant structural deviations

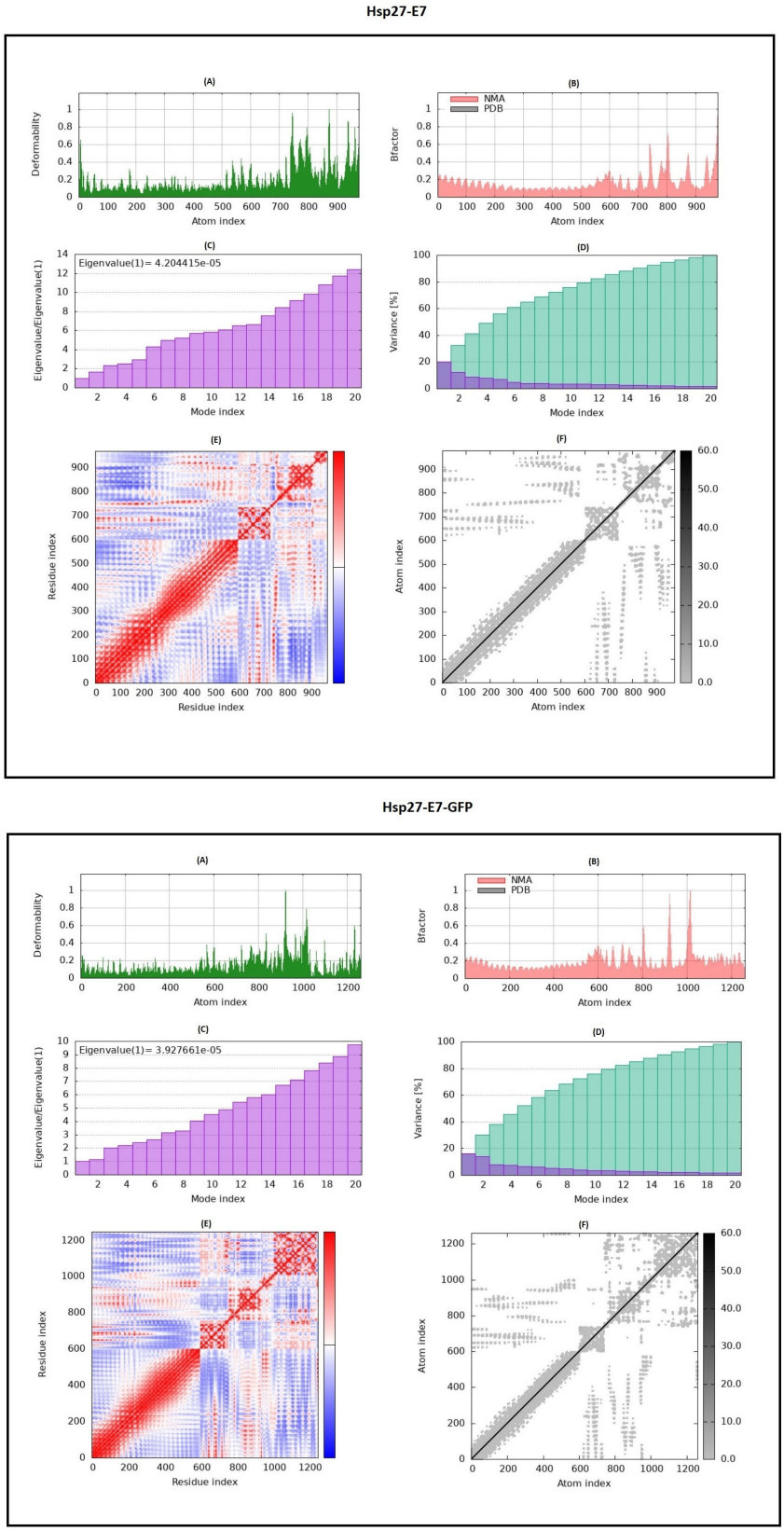

Figure 5. Normal mode analysis of the Hsp27-E7/TLR4 complex or the Hsp27-E7-GFP/TLR4 complex using dihedral coordinates: The ligand-receptor interaction was assessed through comparative analysis of (A) B-factor indices, (B) deformabilities, (C) variance, (D) eigenvalues, (E) covariance of residue indices, and (F) elastic network

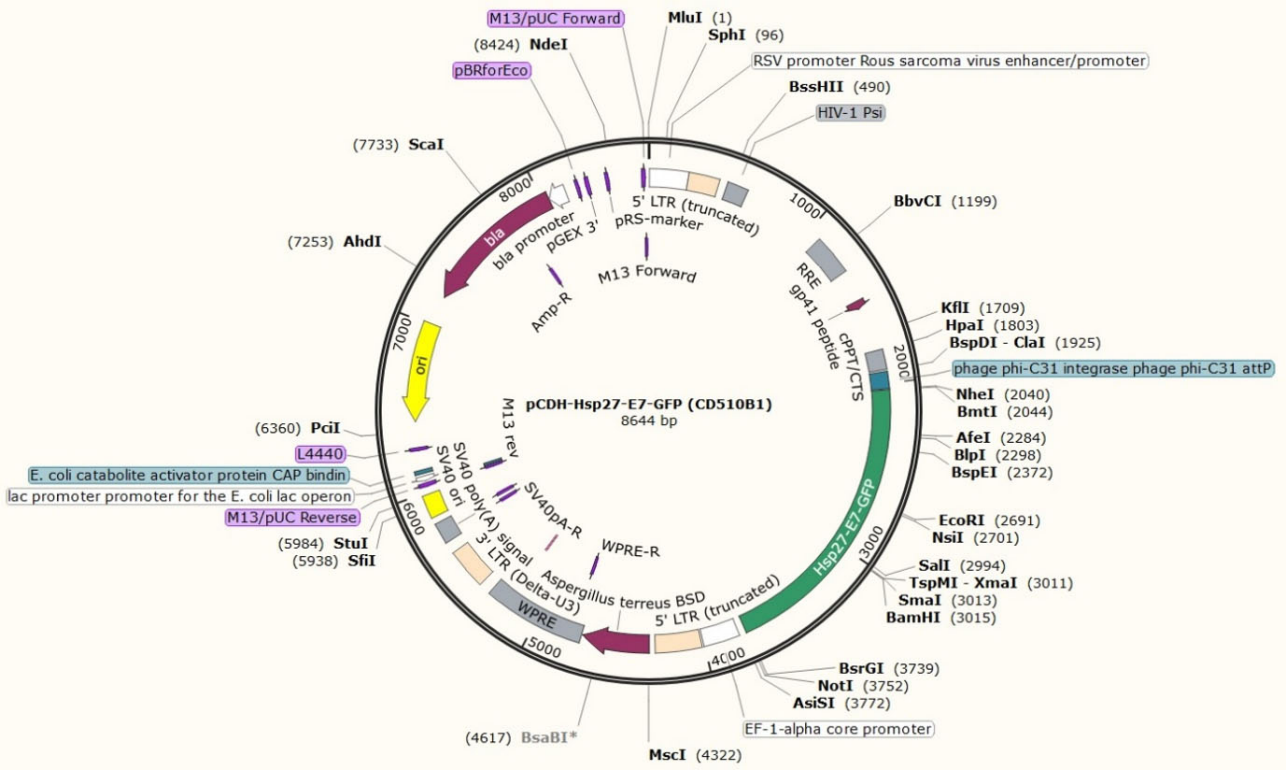

Figure 6. In silico cloning result: Schematic representation of the Hsp27-E7-GFP construct (shown in green) inserted between the NheI (2,040) and NotI (3,752) restriction sites within the pCDH expression vector (shown in black)

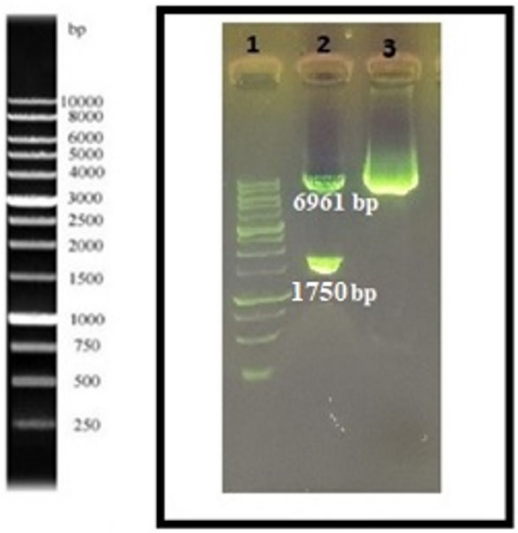

Figure 7. Confirmation of pCDH-Hsp27-E7-GFP (∼6,961 bp for linearized vector and ∼1,750 bp for Hsp27-E7-GFP gene) using NheI/ NotI enzymes: lane 1: DNA Ladder 1 kb (Fermentas), lane 2: The digested plasmid, lane 3: The extracted plasmid

This analysis revealed that both Hsp27-E7-GFP/TLR4 and Hsp27-E7/TLR4 complexes exhibit significant dynamic flexibility, characterized by coupled motions and deformability. Moreover, the linkage of GFP tag to the Hsp27-E7 protein resulted in a lower eigenvalue, indicating potentially reduced overall flexibility. Furthermore, the GFP tag may influence local flexibility within the complex, potentially impacting its interaction with TLR4 or other downstream targets.

3.1.7 *In silico cloning results*

The nucleotide sequence of Hsp27-E7-GFP (∼1,750 bp) was inserted into the multiple cloning site (MCS) of the pCDH vector (∼6,961 bp), positioned between the NheI (2,040) and NotI (3,752) restriction sites (see Figure 6).

3.2 Experimental results

While bioinformatics analysis suggests minimal impact of GFP on the HSP27-E7 structure and binding affinities, it is important to note that the tag could potentially influence the protein's function in vivo. This warrants further in vitro studies as follows. For this purpose, at first, the recombinant pCDH-Hsp27-E7-GFP was prepared and confirmed by the presence of the Hsp27-E7-GFP fusion gene as a clear band of ∼1,750 bp on agarose gel after digestion with specific restriction enzymes (see Figure 7). Moreover, the sequence of Hsp27-E7-GFP fusion gene was validated through Sanger sequencing. Then, the next steps were performed to prepare the engineered exosomes harboring the Hsp27-E7-GFP fusion protein.

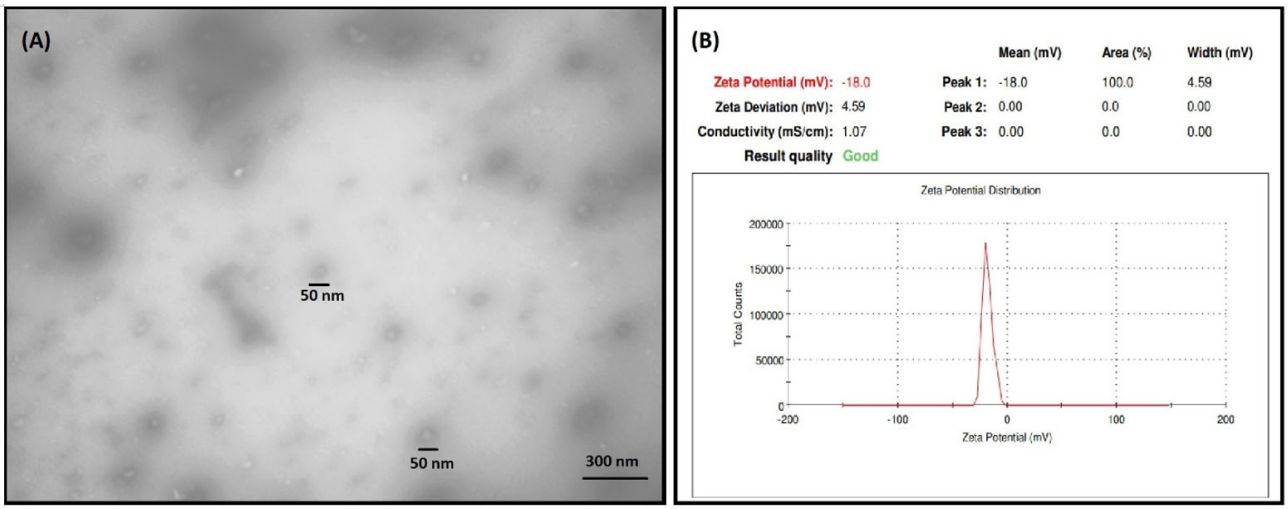

Figure 8. Exosome characterization tests: Characterization of exosomes (Exo) purified from the culture supernatants of TC-1 cells expressing Hsp27-E7-GFP: (A) TEM for determination of size and morphology; (B) Zeta sizer for determination of surface charge/zeta potential

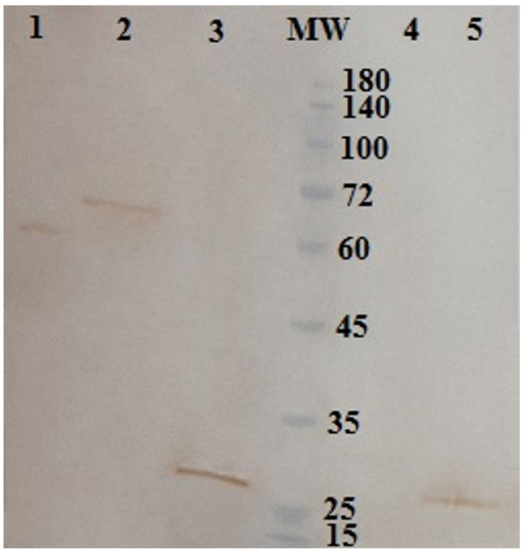

Figure 9. Western blot analysis for identification of exosome markers and loaded proteins: Lanes 1, 2, 5) for Exo-Hsp27-E7-GFP: Lane 1) CD63 marker using anti-CD63 antibody, Lane 2) Hsp27-E7-GFP using anti-GFP antibody, Lane 5) CD9 marker using anti-CD9 antibody; Lane 3: GFP using anti-GFP antibody for Exo-GFP; Lane 4: GFP using anti-GFP antibody for Exo

3.2.1 *Production of the TC-1 cells expressing Hsp27-E7-GFP*

Recombinant lentivirions were produced by transfecting Lenti-X^{TM} HEK cells with pCDH-GFP, pCDH-Hsp27-E7-GFP, and lentiviral packaging vectors using TurboFect^{TM} reagent. Flow cytometry analysis indicated a high transfection efficiency, with 93.04% $\pm$ 1.4% of cells expressing GFP and 81.20% $\pm$ 1.2% expressing Hsp27-E7-GFP after 48 hours. To maximize transduction efficiency, virions were harvested from the supernatants of transfected cells at 24 h, 48 h, and 72 h post-transfection and used to transduce TC-1 cells. Fluorescent microscopy revealed the presence of green fluorescent TC-1 cells 72 hours post-transduction. The flow cytometry results revealed that the percentage of GFP-positive cells was 78.30% $\pm$ 1.5% in the transduced TC-1 cells with lentivirions harboring GFP and 73.26% $\pm$ 1.2% in the transduced TC-1 cells with lentivirions harboring Hsp27-E7-GFP.

3.2.2 *Exosome isolation and characterization*

SEM analysis confirmed the purity and size uniformity of exosomes isolated from non-transduced TC-1 cells using the ExoQuick-TC^{TM} kit. Further characterization using TEM and DLS techniques revealed an average diameter of 50 nm and a specific zeta potential for the exosome populations. TEM provided insights into the size of the exosomes, while DLS measured their surface charge, which is important for understanding the membrane nature of engineered exosomes. All isolated exosomes exhibited a negative surface charge, with values of -13.9 mV for empty exosomes (Exo), -16 mV for Exo-GFP, and -18 mV for Exo-Hsp27-E7-GFP. This negative charge was further enhanced by the inclusion of the Hsp27-E7-GFP protein (see Figure 8).

To fully characterize the isolated exosomes, western blot analysis detected the well-known markers CD63 and CD9, which appeared as distinct bands at 53-60 kDa and 24-27 kDa, respectively. Additionally, the proteins contained within the exosomes were confirmed using an anti-GFP antibody, which showed clear bands at approximately 65 kDa for the Hsp27-E7-GFP fusion protein and around 27 kDa for the

GFP protein (see Figure 9).

3.2.3 *Cytokine secretion from murine APCs incubated with the engineered exosomes*

Based on the obtained data, Exo-Hsp27-E7-GFP (G3) triggered a significantly stronger cytokine secretion from both macrophages and dendritic cells compared to Exo (G1) or Exo-GFP (G2) (see Figure 10).

The incubation of macrophages and dendritic cells with Exo-Hsp27-E7-GFP resulted in enhanced TNF-α production compared to Exo and Exo-GFP ($p < .0001$). Thus, more secretion of TNF-α can related to the loaded fusion protein (Hsp27-E7). The similar result was obtained to secret IL-10 from APCs after incubation with Exo-Hsp27-E7-GFP as compared to Exo and Exo-GFP ($p < .05$). However, Loading GFP in exosomes (Exo-GFP) could significantly increase TNF-α secretion compared to Exo ($p < .05$). However, IFN-γ is commonly not produced by immature DCs and macrophages as reported by published articles.[39,40] It is interesting that TNF-α secreted from DCs is importantly higher than TNF-α secreted from macrophages likely due to different uptake mechanisms.

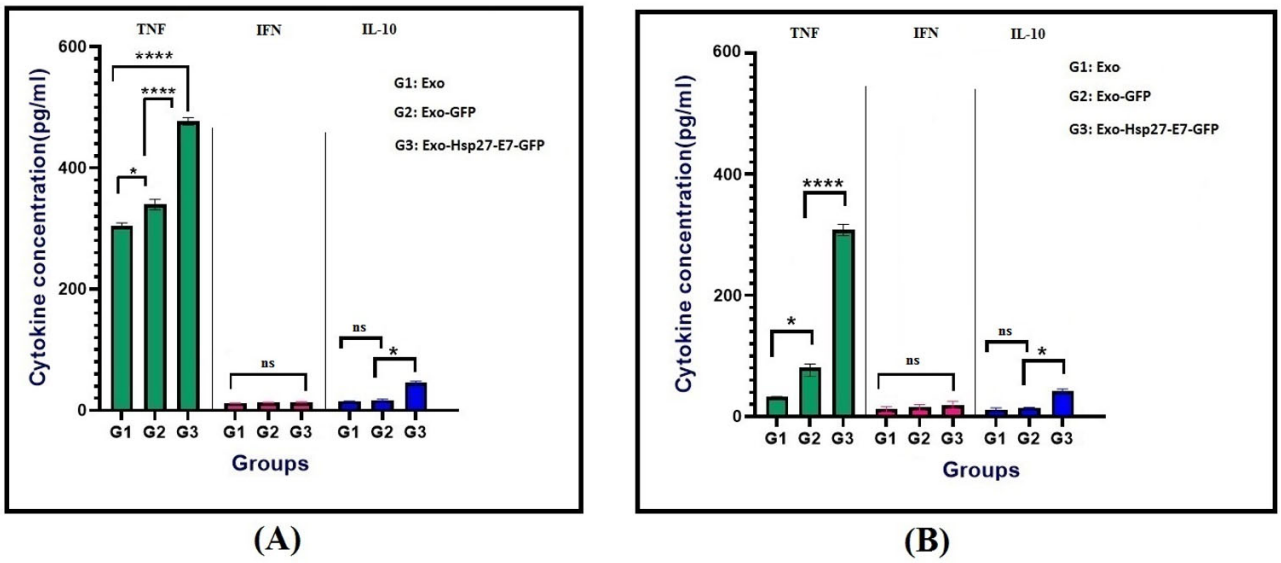

Figure 10. Evaluation of TNF-α, IFN-γ and IL-10 secretion from A) macrophage, B) DC after incubation with Exo, Exo-GFP and Exo-Hsp27-E7-GFP

*All analyses were performed in duplicate for each sample shown as mean absorbance at 450 nm ± SD (*p < .05; ****p < .0001, ns: non-significant)*

4. Discussion

Recent advances in immunotherapy have highlighted the crucial function of heat shock proteins in stimulating immune responses against cancer cells.[41] The development of effective vaccines has led to the engineering of new cell lines as expression platforms, emphasizing the importance of continuous cell lines for scalability and ethical considerations.[42] Given widespread prevalence of HPV infections, it is imperative to enhance the efficiency of therapeutic HPV vaccines.[43] Recombinant proteins often require adjuvants or delivery systems to augment immunogenicity while simultaneously ensuring safety.[44,45] HSPs have proven to be potent immunostimulatory components for vaccine development.[46] Various gene transfer methods, including biological, chemical, and physical approaches, offer distinct advantages, but the ideal method must be efficient, safe, and reproducible.[47] The TC-1 tumor cell line, derived from C57BL/6 mouse lung epithelial cells, serves as a valuable model for preclinical lung cancer and HPV-related studies.[48,49]

The results from the bioinformatics analysis of the Hsp27-E7 and Hsp27-E7-GFP fusion proteins, alongside structural predictions made by the RoseTTAFOLD server, provide a comprehensive understanding of their physicochemical properties and model quality. The selection of Model 1 from RoseTTAFOLD for both constructs highlights the effectiveness of this deep learning-based approach in generating accurate protein models. The Ramachandran plot analysis revealed that 86.3% of residues in the Hsp27-E7 model were in the favored region, while 83.5% of residues in the Hsp27-E7-GFP model were similarly favored. These values indicate a high level of structural a high level of structural integrity, which is essential for the functionality of these proteins. Furthermore, the ERRAT scores obtained (78.235 for Hsp27-E7 and 73.731 for Hsp27-E7-GFP) also underscore the mod-

els' reliability, as scores exceeding 50 are indicative of good model quality.[50] These scores are consistent with other studies that have utilized ERRAT for model validation, reinforcing the notion that high-quality models are essential for downstream applications, such as functional characterization and therapeutic development.

Moreover, disulfide bond connectivity predictions using the DIpro server further supported the structural stability of these constructs.[25,27] In our analysis, the Hsp27-E7 construct revealed 3 disulfide bonds formed by 8 cysteine residues, while the Hsp27-E7-GFP construct showed 4 disulfide bonds involving 10 cysteine residues. On the other hand, molecular dynamics (MD) simulations of the Hsp27-E7-GFP/TLR4 and Hsp27-E7/TLR4 complexes revealed structural stability after approximately four nanoseconds, aligned with similar studies on TLR4 complexes.[51] The radius of gyration (Rg) analysis indicated that the Hsp27-E7/TLR4 complex was more compact than the Hsp27-E7-GFP variant, consistent with other studies reporting variations in Rg values correlating with protein-ligand complex stability.[37] Additionally, the iMODS analysis provided valuable insights into protein dynamics and flexibility, consistent with other studies utilizing this tool for analyzing protein-protein docking and explaining deformability in the main chain.[28,32,52] These analyses collectively reinforced the potential of Hsp27-E7 and Hsp27-E7-GFP as promising antigen candidates.

In this study, TC-1 cells were significantly transduced with lentiviral particles harboring GFP-tagged Hsp27-HPV16 E7 fusion protein. The use of polybrene significantly increased the transduction efficacy.[53] Determining the optimal MOI is crucial for maximizing transduction efficiency. Saltanatpour et al. found that an MOI of 5 resulted in more than 80% GFP-positive cells in the HT29 tumor cell line.[54] Pellinen et al. reported varying efficiencies across cancer cell lines, with the U-87 MG brain cancer cell line achieving the highest efficiency at 94.9%, while the colon cancer cell line CoCa-2 showed only 8.8%.[55] While increasing the MOI can enhance transduction, it may also prolong cell exposure to the virus, potentially reducing target cell lifespan.[56] In our study, we achieved optimal transfer results for the TC-1 cell line using an MOI of 20 and polybrene. Our results demonstrated that engineered TC-1 cells harboring GFP-tagged Hsp27-HPV16 E7 fusion protein achieved high expression levels (73.26% $\pm$ 1.2%). This finding is consistent with previous studies that reported variable transduction efficiencies among different cell lines.[51,52]

The production of multicomponent extracellular vesicles was shown to enhance immunotherapeutic strategies for generating effective antitumor immunity across various cancers.[57] The presence of tumor and self-antigens in these vesicles raises the possibility of autoimmune reactions when they are presented by DCs.[57] To optimize their effectiveness, enhancing the transfer of exosomes to APCs while minimizing potential immunosuppressive effects is essential. This can be achieved by modifying the vesicles with fusion proteins.[57,58] In this study, Hsp27 served as an adjuvant, utilizing its immunomodulatory properties to enhance anti-tumor immunity.[59–61] Our study provides a comprehensive evaluation of engineered exosomes harboring Hsp27-E7-GFP, highlighting their potential as immunotherapeutic agents. It builds upon earlier research that explored GFP-induced immune responses and the application of exosome-based vaccine strategies.[15,62] Combining immunomodulatory molecules with tumor-derived exosomes (TDEs) could enhance anti-tumor immune responses.[63] Hu et al. showed that GFP can elicit immune responses, potentially inducing T cell responses against GFP-expressing cells.[64] Our findings highlight how exosome-bound antigens, like Hsp27-E7-GFP, can further improve immune activation, underscoring the critical importance of both antigen specificity and exosome engineering in eliciting robust immune responses. Moreover, our study emphasized the role of engineered exosomes in enhancing immune responses, demonstrating that exosomes carrying Hsp27-E7-GFP significantly increased TNF-α and IL-10 secretion from dendritic cells and macrophages. The Exo-Hsp27-E7-GFP formulation significantly increased the level of TNF-α compared to Exo, indicating likely a Th1-biased immune response.[65] As mentioned above, binding Hsp27 to TLR4 can activate the release of pro-inflammatory cytokines (e.g., TNF-α) from APCs, which enhances the ability of immune system to target and attack tumor cells. The TNF-α is a key player in mediating immune responses and inflammation during tumor rejection episodes.[66] Its anticancer effects primarily stem from the ability to induce apoptosis in cancer cells, a mechanism that can be leveraged for therapeutic applications in cancer treatment.[67] This is particularly promising for anti-tumor immunity, as Th1 responses are crucial for effective cell-mediated immunity against cancer cells.

Additionally, the DLS analysis revealing a more negative zeta potential for Exo-Hsp27-E7-GFP compared to Exo and Exo-GFP suggests improved stability and reduced aggregation. This characteristic could contribute to enhanced cellular uptake and more effective antigen presentation, potentially leading to stronger immune responses.[68]

Our results are consistent with other studies that underscores the effectiveness of engineered exosomes in enhancing antitumor immunity. In a study performed by Morishita et al., engineered exosomes from the B16BL6 murine melanoma

cell line were produced by transfecting cells with vector expressing streptavidin (SAV) and lactadherin (LA) as a fusion protein on the surface. Then, the CpG DNA (an immune-stimulating adjuvant) were added and incorporated with the engineered exosome. These SAV-LA-CpG exosomes effectively stimulated DCs and presented tumor antigens to the immune system, demonstrating significant antitumor effects.[57] Paola di Bonito et al. were also evaluated the efficiency of engineered exosomes containing the HPV16 E7 antigen and virus-like particles (VLPs). Both approaches effectively stimulated CD8+ T cell immune responses; however, VLPs are considered quite effective immunogens, and also exosomes virtually eliminate the risk of containing harmful viral material.[69] On the other hand, Xie et al. engineered the J558 myeloma cell line to produce exosomes carrying transgenic form of membrane-bound HSP70 and the endogenous P1A tumor antigen. These exosomes exhibited enhanced ability to stimulate DCs for cytokine secretion in vitro and demonstrated potent antitumor effects in vivo.[70]

The study acknowledges several key limitations, primarily its reliance on in vitro experiments, which, while providing valuable insights, cannot fully replicate the complexities of in vivo environments, necessitating further research for validation. Furthermore, while the chosen exosome isolation method was effective, exploring alternative engineering strategies or surface modifications can improve therapeutic efficacy.

In conclusion, our findings underscore the promise of engineered Exo-Hsp27-E7-GFP as a candidate for immunotherapeutic applications such as cancer vaccines. The comprehensive bioinformatics analysis, molecular dynamics simulations, and in vitro studies provide a robust foundation for further research. Subsequent investigations should prioritize on optimizing the exosome engineering process, the exploration of synergistic combinations with other immunomodulatory agents, and the execution of rigorous in vivo studies to evaluate efficacy and safety in animal models. These steps are essential for elucidating the underlying mechanisms of their immunomodulatory effects and for paving the way toward potential clinical applications. Moreover, it is important to note that while our in vitro results are promising, further in vivo studies are necessary to fully understand the efficacy and safety of this approach.

ACKNOWLEDGEMENTS

F. Rezaei was supported by Pasteur Institute of Iran to pursue her study in the Ph.D. thesis.

AUTHORS CONTRIBUTIONS

F.R. performed the experiments and wrote the manuscript. A.A., F.F., S.M.S. and A.B. analysed and validated the data, and revised the manuscript. All authors approved the manuscript.

FUNDING

This research received no external funding.

CONFLICTS OF INTEREST DISCLOSURE

The authors declare they have no conflicts of interest.

INFORMED CONSENT

Not applicable.

ETHICS STATEMENT

In vitro studies were conducted in strict adherence to approved protocols and in compliance with the highest standards of animal care at the Pasteur Institute of Iran. This study was conducted in accordance with ethics code IR.PII.REC.1400.025.

ETHICS APPROVAL

The Publication Ethics Committee of the Sciedu Press. The journal's policies adhere to the Core Practices established by the Committee on Publication Ethics (COPE).

PROVENANCE AND PEER REVIEW

Not commissioned; externally double-blind peer reviewed.

DATA AVAILABILITY STATEMENT

The data that support the findings of this study are available in the manuscript.

DATA SHARING STATEMENT

Not applicable.

REFERENCES

[1] Okunade KS. Human papillomavirus and cervical cancer. Journal of Obstetrics and Gynaecology. 2020; 40(5): 602-608. PMid: 31500479. https://doi.org/10.1080/01443615.2019.1634030

[2] Ye J, Zheng L, He Y, et al. Human papillomavirus associated cervical lesion: pathogenesis and therapeutic interventions. MedComm. 2023; 4(5): e368. PMid: 37719443. https://doi.org/10.1002/mco2.368

[3] Yusuf M. Perspectives on cervical cancer: Insights into screening methodology and challenges. Cancer Screening and Prevention. 2024; 3(1): 52-60. https://doi.org/10.14218/CSP.2023.00041

[4] Rathod S, Potdar J, Gupta A, et al. Empowering women's health: insights into HPV vaccination and the prevention of invasive cervical cancer. Cureus. 2023; 15(11): e49523. https://doi.org/10.7759/cureus.49523

[5] Yim EK, Park JS. The role of HPV E6 and E7 oncoproteins in HPV-associated cervical carcinogenesis. Cancer research and treatment: official journal of Korean Cancer Association. 2005; 37(6): 319-324. PMid: 19956366. https://doi.org/10.4143/crt.2005.37.6.319

[6] Kamolratanakul S, Pitisuttithum P. Human papillomavirus vaccine efficacy and effectiveness against cancer. Vaccines. 2021; 9(12): 1413. PMid: 34960159. https://doi.org/10.3390/vaccines9121413

[7] Han L, Zhang B. Can prophylactic HPV vaccination reduce the recurrence of cervical lesions after surgery? Review and prospect. Infectious Agents and Cancer. 2023; 18(1): 66. PMid: 37898754. https://doi.org/10.1186/s13027-023-00547-2

[8] Yan F, Cowell LG, Tomkies A, et al. Therapeutic vaccination for HPV-mediated cancers. Current Otorhinolaryngology Reports. 2023; 11(1): 44-61. PMid: 36743978. https://doi.org/10.1007/s40136-023-00443-8

[9] Tiwari P, Yadav K, Shukla RP, et al. Extracellular vesicles-powered immunotherapy: Unleashing the potential for safer and more effective cancer treatment. Archives of Biochemistry and Biophysics. 2024; 756: 110022. PMid: 38697343. https://doi.org/10.1016/j.abb.2024.110022

[10] Mittal S, Gupta P, Chaluvally-Raghavan P, et al. Emerging role of extracellular vesicles in immune regulation and cancer progression. Cancers. 2020; 12(12): 3563. PMid: 33260606. https://doi.org/10.3390/cancers12123563

[11] Saito RF, Machado CML, Lomba ALO, et al. Heat shock proteins mediate intercellular communications within the tumor microenvironment through extracellular vesicles. Applied Biosciences. 2024; 3(1): 45-58. https://doi.org/10.3390/applbiosci3010003

[12] Shi C, Ulke-Lemée A, Deng J, et al. Characterization of heat shock protein 27 in extracellular vesicles: a potential anti-inflammatory therapy. The FASEB Journal. 2019; 33(2): 1617-1630. PMid: 30188755. https://doi.org/10.1096/fj.201800987R

[13] Barros FM, Carneiro F, Machado JC, et al. Exosomes and immune response in cancer: friends or foes? Frontiers in Immunology. 2018; 9: 730. PMid: 29696022. https://doi.org/10.3389/fimmu.2018.00730

[14] Regimbeau M, Abrey J, Vautrot V, et al., editors. Heat shock proteins and exosomes in cancer theranostics. Elsevier: Seminars in Cancer Biology; 2022. PMid: 34343652. https://doi.org/10.1016/j.semcancer.2021.07.014

[15] Ansari AM, Ahmed AK, Matsangos AE, et al. Cellular GFP toxicity and immunogenicity: potential confounders in in vivo cell tracking experiments. Stem Cell Reviews and Reports. 2016; 12: 553-559. PMid: 27435468. https://doi.org/10.1007/s12015-016-9670-8

[16] Grzelak CA, Goddard ET, Lederer EE, et al. Elimination of fluorescent protein immunogenicity permits modeling of metastasis in immune-competent settings. Cancer Cell. 2022; 40(1): 1-2. PMid: 34861158. https://doi.org/10.1016/j.ccell.2021.11.004

[17] Lee JE, Chung Y, Rhee S, et al. Untold story of human cervical cancers: HPV-negative cervical cancer. BMB reports. 2022; 55(9): 429. PMid: 35725012. https://doi.org/10.5483/BMBRep.2022.55.9.042

[18] Rezaei F, Namvar A, Akbari E, et al. Immunoinformatics studies of heat shock proteins 27 and 70: Development of potent therapeutic vaccine constructs against human papillomavirus-related cancers. Heliyon. 2023; 9(8): e19261. PMid: 37664744. https://doi.org/10.1016/j.heliyon.2023.e19261

[19] Du Z, Su H, Wang W, et al. The trRosetta server for fast and accurate protein structure prediction. Nature Protocols. 2021; 16(12): 5634-5651. PMid: 34759384. https://doi.org/10.1038/s41596-021-00628-9

[20] Heo L, Park H, Seok C. GalaxyRefine: Protein structure refinement driven by side-chain repacking. Nucleic Acids Research. 2013; 41(W1): W384-W388. PMid: 23737448. https://doi.org/10.1093/nar/gkt458

[21] Laskowski RA, MacArthur MW, Thornton JM. PROCHECK: validation of protein-structure coordinates. International Tables for Crystallography. 2012; F (21.4): 684-687 https://doi.org/10.1107/97809553602060000882

[22] Colovos C, Yeates TO. Verification of protein structures: patterns of nonbonded atomic interactions. Protein science. 1993; 2(9): 1511-1519. PMid: 8401235. https://doi.org/10.1002/pro.5560020916

[23] Gasteiger E, Hoogland C, Gattiker A, et al. Protein identification and analysis tools on the ExPASy server. Springer; 2005. https://doi.org/10.1385/1-59259-890-0:571

[24] Hebditch M, Carballo-Amador MA, Charonis S, et al. Protein-Sol: a web tool for predicting protein solubility from sequence. Bioinformatics. 2017; 33(19): 3098-3100. PMid: 28575391. https://doi.org/10.1093/bioinformatics/btx345

[25] Cheng J, Saigo H, Baldi P. Large-scale prediction of disulphide bridges using kernel methods, two-dimensional recursive neural networks, and weighted graph matching. Proteins: Structure, Function, and Bioinformatics. 2006; 62(3): 617-629. PMid: 16320312. https://doi.org/10.1002/prot.20787

[26] Cheng J, Vullo A, Baldi P. Large-scale prediction of disulphide bond connectivity. Advances in Neural Information Processing Systems. 2004; 17: 1-8.

[27] Cheng J, Randall AZ, Sweredoski MJ, et al. SCRATCH: a protein structure and structural feature prediction server. Nucleic Acids Research. 2005; 33(suppl_2): W72-W76. PMid: 15980571. https://doi.org/10.1093/nar/gki396

[28] Lopéz-Blanco JR, Garzón JI, Chacón P. iMod: multipurpose normal mode analysis in internal coordinates. Bioinformatics. 2011; 27(20): 2843-2850. PMid: 21873636. https://doi.org/10.1093/bioinformatics/btr497

[29] Bauer JA, Pavlović J, Bauerová-Hlinková V. Normal mode analysis as a routine part of a structural investigation. Molecules. 2019; 24(18): 3293. PMid: 31510014. https://doi.org/10.3390/molecules24183293

[30] Sikic K, Jeren B, Tomic S, editors. Identifying Protein Flexibility by NMA. BIOCOMP. 2008; 927-933.

[31] Hospital A, Goñi JR, Orozco M, et al. Molecular dynamics simulations: advances and applications. Advances and Applications

in Bioinformatics and Chemistry. 2015; 37-47. PMid: 26604800. https://doi.org/10.2147/AABC.S70333

[32] López-Blanco JR, Aliaga JI, Quintana-Ortí ES, et al. iMODS: internal coordinates normal mode analysis server. Nucleic Acids Research. 2014; 42(W1): W271-W276. PMid: 24771341. https://doi.org/10.1093/nar/gku339

[33] Zhang B, Metharom P, Jullie H, et al. The significance of controlled conditions in lentiviral vector titration and in the use of multiplicity of infection (MOI) for predicting gene transfer events. Genetic Vaccines and Therapy. 2004; 2: 1-10. PMid: 15291957. https://doi.org/10.1186/1479-0556-2-6

[34] Milani A, Agi E, Pouriayevali MH, et al. Different dendritic cells-based vaccine constructs influence HIV-1 antigen-specific immunological responses and cytokine generation in virion-exposed splenocytes. International Immunopharmacology. 2022; 113: 109406. PMid: 36461600. https://doi.org/10.1016/j.intimp.2022.109406

[35] Messaoudi A, Belguith H, Ben Hamida J. Homology modeling and virtual screening approaches to identify potent inhibitors of VEB-1 β-lactamase. Theoretical Biology and Medical Modelling. 2013; 10: 1-10. PMid: 23547944. https://doi.org/10.1186/1742-4682-10-22

[36] Cuspoca AF, Díaz LL, Acosta AF, et al. An immunoinformatics approach for sars-cov-2 in latam populations and multi-epitope vaccine candidate directed towards the world's population. Vaccines. 2021; 9(6): 581. PMid: 34205992. https://doi.org/10.3390/vaccines9060581

[37] Rahimi M, Taghdir M, Abasi Joozdani F. Dynamozones are the most obvious sign of the evolution of conformational dynamics in HIV-1 protease. Scientific Reports. 2023; 13(1): 14179. PMid: 37648682. https://doi.org/10.1038/s41598-023-40818-x

[38] Huynh T, Smith JC, Sanson A. Protein unfolding transitions in an intrinsically unstable annexin domain: Molecular dynamics simulation and comparison with nuclear magnetic resonance data. Biophysical Journal. 2002; 83(2): 681-698. PMid: 12124256. https://doi.org/10.1016/S0006-3495(02)75200-4

[39] Brady MT, Lee J, Ferrone S, et al. Interferon-γ secretion by t (9; 22) acute lymphoblastic leukemia-derived dendritic cells. Leukemia Research. 2011; 35(2): 275-277. PMid: 20943267. https://doi.org/10.1016/j.leukres.2010.09.003

[40] Darwich L, Coma G, Peña R, et al. Secretion of interferon-γ by human macrophages demonstrated at the single-cell level after costimulation with interleukin (IL)-12 plus IL-18. Immunology. 2009; 126(3): 386-393. PMid: 18759749. https://doi.org/10.1111/j.1365-2567.2008.02905.x

[41] Yang S, Xiao H, Cao L. Recent advances in heat shock proteins in cancer diagnosis, prognosis, metabolism and treatment. Biomedicine & Pharmacotherapy. 2021; 142: 112074. PMid: 34426258. https://doi.org/10.1016/j.biopha.2021.112074 PMid: 34426258.

[42] Demirden SF, Kimiz-Gebologlu I, Oncel SS. Animal cell lines as expression platforms in viral vaccine production: A post covid-19 perspective. ACS Omega. 2024; 9(15): 16904-16926. PMid: 38645343. https://doi.org/10.1021/acsomega.3c10484

[43] Mo Y, Ma J, Zhang H, et al. Prophylactic and therapeutic HPV vaccines: current scenario and perspectives. Frontiers in Cellular and Infection Microbiology. 2022; 12: 909223. PMid: 35860379. https://doi.org/10.3389/fcimb.2022.909223

[44] Milani A, Basirnejad M, Bolhassani A. Heat-shock proteins in diagnosis and treatment: An overview of different biochemical and immunological functions. Immunotherapy. 2019; 11(3): 215-239. PMid: 30730280. https://doi.org/10.2217/imt-2018-0105

[45] Robert J. Evolution of heat shock protein and immunity. Developmental & Comparative Immunology. 2003; 27(6-7): 449-464. PMid: 12697304. https://doi.org/10.1016/S0145-305X(02)00160-X

[46] Shevtsov M, Multhoff G. Heat shock protein-peptide and HSP-based immunotherapies for the treatment of cancer. Frontiers in immunology. 2016;7:180087. PMid: 27199993. https://doi.org/10.3389/fimmu.2016.00171

[47] Kim TK, Eberwine JH. Mammalian cell transfection: the present and the future. Analytical and Bioanalytical Chemistry. 2010; 397: 3173-3178. PMid: 20549496. https://doi.org/10.1007/s00216-010-3821-6

[48] Sadraeian M, Mansoorkhani MJK, Mohkam M, et al. Prevention and inhibition of TC-1 cell growth in tumor bearing mice by HPV16 E7 protein in fusion with Shiga toxin B-subunit from shigella dysenteriae. Cell Journal (Yakhteh). 2013; 15(2): 176.

[49] Fazeli M, Soleimanjahi H, Ghaemi A, et al. Efficacy of HPV-16 E7 based vaccine in a TC-1 tumoric animal model of cervical cancer. Cell Journal (Yakhteh). 2011; 12(4): 483-488.

[50] Williams ME. HIV-1 vif protein sequence variations in South African people living with HIV and their influence on Vif-APOBEC3G interaction. European Journal of Clinical Microbiology & Infectious Diseases. 2024; 43(2): 325-338. PMid: 38072879. https://doi.org/10.1007/s10096-023-04728-0

[51] Patra MC, Kwon HK, Batool M, et al. Computational insight into the structural organization of full-length Toll-like receptor 4 dimer in a model phospholipid bilayer. Frontiers in Immunology. 2018; 9: 489. PMid: 29593733. https://doi.org/10.3389/fimmu.2018.00489

[52] Zaib S, Rana N, Hussain N, et al. Designing multi-epitope monkeypox virus-specific vaccine using immunoinformatics approach. Journal of Infection and Public Health. 2023; 16(1): 107-116. PMid: 36508944. https://doi.org/10.1016/j.jiph.2022.11.033

[53] Steffens S, Tebbets J, Kramm CM, et al. Transduction of human glial and neuronal tumor cells with different lentivirus vector pseudotypes. Journal of Neuro-oncology. 2004; 70: 281-288. PMid: 15662969. https://doi.org/10.1007/s11060-004-6046-8

[54] Saltanatpour Z, Kadivar M, Johari B, et al. Transduction of an optimized recombinant lentivirus expressing E-cadherin shRNA resulted in stable downregulation of CDH1 gene and obvious cell morphological change in the human colorectal cancer cell line HT29. Intern J Med Res Health Sci. 2016; 5(11): 87-93.

[55] Pellinen R, Hakkarainen T, Wahlfors T, et al. Cancer cells as targets for lentivirus-mediated gene transfer and gene therapy. International Journal of Oncology. 2004; 25(6): 1753-1762. PMid: 15547714. https://doi.org/10.3892/ijo.25.6.1753

[56] Zhao XY, Xu QL, Zhao XD, et al. Enhancing lentiviral vector transduction efficiency for facilitating gene therapy. China Biotechnology. 2021; 41(8): 52-58.

[57] Morishita M, Takahashi Y, Matsumoto A, et al. Exosome-based tumor antigens-adjuvant co-delivery utilizing genetically engineered tumor cell-derived exosomes with immunostimulatory CpG DNA. Biomaterials. 2016; 111: 55-65. PMid: 27723556. https://doi.org/10.1016/j.biomaterials.2016.09.031

[58] Di Bonito P, Ridolfi B, Columba-Cabezas S, et al. HPV-E7 delivered by engineered exosomes elicits a protective CD8+ T cell-mediated immune response. Viruses. 2015; 7(3): 1079-1099. PMid: 25760140. https://doi.org/10.3390/v7031079

[59] Chen W, Wang J, Shao C, et al. Efficient induction of antitumor T cell immunity by exosomes derived from heat-shocked lymphoma cells. European Journal of Immunology. 2006; 36(6): 1598-1607. PMid: 16708399. https://doi.org/10.1002/eji.200535501

[60] Zhang M, Jin K, Gao L, et al. Methods and technologies for exosome isolation and characterization. Small Methods. 2018; 2(9): 1800021. https://doi.org/10.1002/smtd.201800021

[61] Somu P, Paul S. Inter-relationship between the inflammation and heat shock protein in cancer development: A possible target for diagnosis and cancer immunotherapy. Heat Shock Proteins in Human Diseases. 2021; 1-29. https://doi.org/10.1007/7515_2020_19

[62] Cao J, Lv G, Wei F. Engineering exosomes to reshape the immune microenvironment in breast cancer: Molecular insights and therapeutic opportunities. Clinical and Translational Medicine. 2024; 14(4): e1645. PMid: 38572668. https://doi.org/10.1002/ctm2.1645

[63] Santos P, Almeida F. Exosome-based vaccines: history, current state, and clinical trials. Frontiers in Immunology. 2021; 12: 711565. PMid: 34335627. https://doi.org/10.3389/fimmu.2021.711565

[64] Hu K, McKay PF, Samnuan K, et al. Presentation of antigen on extracellular vesicles using transmembrane domains from viral glycoproteins for enhanced immunogenicity. Journal of Extracellular Vesicles. 2022; 11(3): e12199. PMid: 35233930. https://doi.org/10.1002/jev2.12199

[65] Morosini M, Meloni F, Uccelli M, et al. Ex vivo evaluation of PPD-specific IFN-γ or IL-5 secreting cells in the peripheral blood and lungs of patients with tuberculosis. The International Journal of Tuberculosis and Lung Disease. 2005; 9(7): 753-759.

[66] Jang DI, Lee AH, Shin HY, et al. The role of tumor necrosis factor alpha (TNF-α) in autoimmune disease and current TNF-α inhibitors in therapeutics. International Journal of Molecular Sciences. 2021; 22(5): 2719. PMid: 33800290. https://doi.org/10.3390/ijms22052719

[67] Wang X, Lin Y. Tumor necrosis factor and cancer, buddies or foes? 1. Acta Pharmacologica Sinica. 2008; 29(11): 1275-1288. PMid: 18954521. https://doi.org/10.1111/j.1745-7254.2008.00889.x

[68] Midekessa G, Godakumara K, Ord J, et al. Zeta potential of extracellular vesicles: toward understanding the attributes that determine colloidal stability. ACS Omega. 2020; 5(27): 16701-16710. PMid: 32685837. https://doi.org/10.1021/acsomega.0c01582

[69] Di Bonito P, Ridolfi B, Columba-Cabezas S, et al. HPV-E7 delivered by engineered exosomes elicits a protective CD8+ T cell-mediated immune response. Viruses. 2015; 7(3): 1079-1099. PMid: 25760140. https://doi.org/10.3390/v7031079

[70] Xie Y, Bai O, Zhang H, et al. Membrane-bound HSP70-engineered myeloma cell-derived exosomes stimulate more efficient CD8(+) CTL- and NK-mediated antitumour immunity than exosomes released from heat-shocked tumour cells expressing cytoplasmic HSP70. Journal of Cellular and Molecular Medicine. 2010; 14(11): 2655-2666. PMid: 19627400. https://doi.org/10.1111/j.1582-4934.2009.00851.x